

Topological Kirchhoff Law and Bulk-Edge Correspondence for Valley-Chern and Spin-Valley-Chern Numbers

Motohiko Ezawa

Department of Applied Physics, University of Tokyo, Hongo 7-3-1, 113-8656, Japan

The valley-Chern and spin-valley-Chern numbers are the key concepts in valleytronics. They are topological numbers in the Dirac theory but not in the tight-binding model. We analyze the bulk-edge correspondence between the two phases which have the same Chern and spin-Chern numbers but different valley-Chern and spin-valley-Chern numbers. The edge state between them is topologically trivial in the tight-binding model but is shown to be as robust as the topological edge. We construct Y-junctions made of topological edges. They satisfy the topological Kirchhoff law, where the topological charges are conserved at the junction. We may interpret a Y-junction as a scattering process of particles which have four topological numbers. It would be a milestone of future topological electronics.

Topological insulator is one of the most fascinating concepts found in this decade[1, 2]. It is characterized by topological numbers such as the Chern (C) number and the \mathbb{Z}_2 index. When the spin s_z is a good quantum number, the spin-Chern (C_s) number replaces the role of the \mathbb{Z}_2 index[3–5]. We consider honeycomb lattice systems. Electrons reside either in the K or K' valley in the low-energy Dirac theory. Accordingly we can define the valley-Chern (C_v) number[18–20] and the spin-valley-Chern (C_{sv}) number[18] in the Dirac theory. This valley degree of freedom leads to valleytronics[6–17]. However, the C_v and C_{sv} numbers are ill-defined in the tight-binding model because the topological numbers are defined by the summation of Berry curvatures over the entire Brillouin zone. Namely, a state is indexed by the two topological numbers in the tight-binding model, while it is indexed by the four topological numbers in the Dirac theory.

There are four independent spin-valley dependent Chern numbers in the Dirac theory of honeycomb systems. Each Chern number can be controlled independently by changing the sign of spin-valley dependent Dirac masses. There are 16 types of topological insulators, as shown in the table I. They are quantum anomalous Hall (QAH) insulator, four types of spin-polarized QAH (SQAH) insulators, quantum spin Hall (QSH) insulator and the band insulator with charge-density-wave (CDW) or antiferromagnetic (AF) order. The CDW and AF insulators are regarded trivial in the tight-binding model.

In this paper, we study the bulk-edge correspondence with respect to the C_v and C_{sv} numbers by examining the boundary of two insulators which have the same C and C_s numbers but different C_v and C_{sv} numbers. First we show that gapless edge states appear though they are trivial in the tight-binding model. Furthermore, we show that they are as robust as the topologically protected edges.

We propose a topological electronics based on the edge states in the Dirac theory. We are able to assign four topological numbers to each edge state. By joining three different topological insulators at one point, we can construct a Y-junction made of topological edge states. The edge states at the junction satisfy the conservation of four topological numbers, which we call the topological Kirchhoff law. We can change the connectivity of edge states by changing the

	C_{\uparrow}^K	$C_{\uparrow}^{K'}$	C_{\downarrow}^K	$C_{\downarrow}^{K'}$	C	$2C_s$	C_v	$2C_{sv}$
QAH	1/2	1/2	1/2	1/2	2	0	0	0
SQAH ₁	1/2	1/2	1/2	-1/2	1	1	1	-1
SQAH ₂	1/2	-1/2	1/2	1/2	1	1	-1	1
SQAH ₃	1/2	1/2	-1/2	1/2	1	-1	1	1
SQAH ₄	-1/2	1/2	1/2	1/2	1	-1	-1	-1
QSH	1/2	-1/2	1/2	-1/2	0	2	0	0
CDW	1/2	1/2	-1/2	-1/2	0	0	2	0
AF	1/2	-1/2	-1/2	1/2	0	0	0	2

TABLE I: Corresponding to the spin and valley degrees of freedom, there are 4 Chern numbers $C_{s_z}^{\eta}$, each of which takes $\pm\frac{1}{2}$. Equivalently they are given by the Chern (C), spin-Chern (C_s), valley-Chern (C_v) and spin-valley-Chern (C_{sv}) numbers. Hence there are 16 states indexed by them, among which 8 states are explicitly displayed. The other 8 states are the conjugate states such as QAH* whose topological numbers are given by $-C_{s_z}^{\eta}$.

topological property of bulk insulators, for instance, by applying electric field. The process may be interpreted as a pair annihilation of two Y-junctions.

Hamiltonian: The honeycomb lattice consists of two sublattices made of A and B sites. We consider a buckled system with the layer separation 2ℓ between these two sublattices. The states near the Fermi energy are π orbitals residing near the K and K' points at opposite corners of the hexagonal Brillouin zone. The low-energy dynamics in the K and K' valleys is described by the Dirac theory. In what follows we use notations $s_z = \uparrow, \downarrow$, $t_z = A, B$, $\eta = K, K'$ in indices while $s_z^{\alpha} = \pm 1$ for $\alpha = \uparrow, \downarrow$, $t_z^i = \pm 1$ for $i = A, B$, and $\eta_i = \pm 1$ for $i = K, K'$ in equations. We also use the Pauli matrices σ_a and τ_a for the spin and the sublattice pseudospin, respectively.

We have previously proposed a generic Hamiltonian for honeycomb systems[21], which contains eight interaction terms mutually commutative in the Dirac limit. Among them four contribute to the Dirac mass. The other four contribute to the shift of the energy spectrum. We are able to make a full control of the Dirac mass and the energy shift independently at each spin and valley by varying these parameters, and materialize various topological phases[22, 23].

By taking those affecting the Dirac mass, the tight-binding model is given by[21, 24, 25],

$$\begin{aligned}
H = & -t \sum_{\langle i,j \rangle \alpha} c_{i\alpha}^\dagger c_{j\alpha} + i \frac{\lambda_{SO}}{3\sqrt{3}} \sum_{\langle\langle i,j \rangle\rangle \alpha\beta} \nu_{ij} c_{i\alpha}^\dagger \sigma_{\alpha\beta}^z c_{j\beta} \\
& -\lambda_V \sum_{i\alpha} \mu_i c_{i\alpha}^\dagger c_{i\alpha} + i \frac{\lambda_\Omega}{3\sqrt{3}} \sum_{\langle\langle i,j \rangle\rangle \alpha\beta} \nu_{ij} c_{i\alpha}^\dagger c_{j\beta} \\
& +\lambda_{SX} \sum_{i\alpha} \mu_i c_{i\alpha}^\dagger \sigma_{\alpha\alpha}^z c_{i\alpha}, \quad (1)
\end{aligned}$$

where $c_{i\alpha}^\dagger$ creates an electron with spin polarization α at site i , and $\langle i, j \rangle / \langle\langle i, j \rangle\rangle$ run over all the nearest/next-nearest neighbor hopping sites. We explain each term. The first term represents the nearest-neighbor hopping with the transfer energy t . The second term represents the SO coupling[24] with λ_{SO} . The third term is the staggered sublattice potential term[26] with $\lambda_V = \ell E_z$ in electric field E_z . The fourth term is the Haldane term[27] with λ_Ω . The fifth term represents the antiferromagnetic exchange magnetization[21, 28] with λ_{SX} .

We give typical sample parameters though we treat them as free parameters. Silicene is a good candidate, where $t = 1.6\text{eV}$, $\lambda_{SO} = 3.9\text{meV}$ and $\ell = 0.23\text{\AA}$. The Haldane term might be induced by the photo-irradiation, where $\lambda_\Omega = \hbar v_F^2 \mathcal{A}^2 \Omega^{-1}$ with Ω the frequency and \mathcal{A} the dimensionless intensity[23, 29, 30]. The antiferromagnetic exchange magnetization might be induced by certain proximity effects. The second candidate is provskite transition-metal-oxide grown on [111]-direction, which has antiferromagnetic order intrinsically[31]. This material has also the buckled structure as in the case of silicene. Parameters are $t \approx 0.2\text{eV}$, $\lambda_{SO} = 7.3\text{meV}$, $\lambda_V = \ell E_z$, $\lambda_{SX} = 141\text{meV}$ for LaCrAgO.

The low-energy Hamiltonian is described by[21]

$$\begin{aligned}
H_\eta = & \hbar v_F (\eta k_x \tau_x + k_y \tau_y) + \lambda_{SO} \sigma_z \eta \tau_z \\
& -\lambda_V \tau_z + \lambda_\Omega \eta \tau_z + \lambda_{SX} \sigma_z \tau_z, \quad (2)
\end{aligned}$$

where $v_F = \frac{\sqrt{3}}{2\hbar} at$ is the Fermi velocity. The coefficient of τ_z is the mass of Dirac fermions in the Hamiltonian,

$$\Delta_{s_z}^\eta = \eta s_z \lambda_{SO} - \lambda_V + \eta \lambda_\Omega + s_z \lambda_{SX}. \quad (3)$$

The band gap is given by $2|\Delta_{s_z}^\eta|$.

Topological numbers: We consider the systems where the spin s_z is a good quantum number. The summation of the Berry curvature over all occupied states of electrons with spin s_z in the Dirac valley K_η yields[1, 2, 32]

$$\mathcal{C}_{s_z}^\eta = \frac{\eta}{2} \text{sgn}(\Delta_{s_z}^\eta). \quad (4)$$

There are four independent spin-valley dependent Dirac masses determined by the four parameters λ_{SO} , λ_V , λ_Ω and λ_{SX} . Accordingly, we can define

$$\mathcal{C} = \mathcal{C}_\uparrow^K + \mathcal{C}_\uparrow^{K'} + \mathcal{C}_\downarrow^K + \mathcal{C}_\downarrow^{K'}, \quad (5)$$

$$\mathcal{C}_s = \frac{1}{2}(\mathcal{C}_\uparrow^K + \mathcal{C}_\uparrow^{K'} - \mathcal{C}_\downarrow^K - \mathcal{C}_\downarrow^{K'}), \quad (6)$$

and

$$\mathcal{C}_v = \mathcal{C}_\uparrow^K - \mathcal{C}_\uparrow^{K'} + \mathcal{C}_\downarrow^K - \mathcal{C}_\downarrow^{K'}, \quad (7)$$

$$\mathcal{C}_{sv} = \frac{1}{2}(\mathcal{C}_\uparrow^K - \mathcal{C}_\uparrow^{K'} - \mathcal{C}_\downarrow^K + \mathcal{C}_\downarrow^{K'}). \quad (8)$$

It is to be emphasized that \mathcal{C}_v and \mathcal{C}_{sv} are not defined in the tight-binding model.

The possible sets of topological numbers are $(0, 0)$, $(2, 0)$, $(0, 1)$, $(1, \frac{1}{2})$, $(1, -\frac{1}{2})$ up to the overall sign \pm in the tight-binding model. They are the trivial, QAH, QSH and two types of SQAH insulators, respectively. They are further classified into subsets according to the valley degree of freedom in the Dirac theory. Trivial insulators are divided into two; one with CDW order and the other with AF orders[21]. Each type of SQAH insulators are divided into two: There are four types in all, which we denote by SQAH $_i$ with $i = 1, 2, 3, 4$. All of them are summarized in Table I.

Bulk-edge correspondence: The most convenient way to determine the topological charges is to employ the bulk-edge correspondence. When there are two topological distinct phases, a topological phase transition may occur between them. It is generally accepted that the band gap must close at the topological phase transition point since the topological number cannot change its quantized value without gap closing. Note that the topological number is only defined in the gapped system and remains unchanged for any adiabatic process. Alternatively, we may consider a junction separating two different topological phases in a single honeycomb system[26]. Gapless edge modes must appear along the boundary. We may as well analyze the energy spectrum of a nanoribbon in a topological phase, because the boundary of the nanoribbon separates a topological state and the vacuum whose topological numbers are zero: See Fig.1(a).

CDW-AF junction: We first investigate the trivial insulator in the tight-binding model, which consists of two subsets (CDW and AF) in the Dirac theory. It is well known that a nanoribbon made of either the CDW insulator or the AF insulator has no gapless edge modes, as is regarded to be a demonstration of their triviality: See Fig.1(b) and (c). One may wonder how they can be topological in the Dirac theory without gapless edge modes in view of the bulk-edge correspondence. The answer to this problem is that the \mathcal{C}_v and \mathcal{C}_{sv} numbers are not defined in the vacuum. Indeed, only the charge and the spin are well defined to be zero in the vacuum. Note that the gap needs not close at such a boundary because \mathcal{C}_v and \mathcal{C}_{sv} are defined only inside of the nanoribbon. This explains the absence of gapless edge modes in Fig.1(b) and (c).

We investigate the junction made of the CDW and AF insulators, whose topological numbers are $(\mathcal{C}, \mathcal{C}_s, \mathcal{C}_v, \mathcal{C}_{sv}) = (0, 0, 2, 0)$ and $(0, 0, 0, 2)$, respectively. On one hand, we expect no gapless edge modes in the tight-binding model. On the other hands, there should be gapless edge modes in the Dirac theory. We ask how these two properties are compatible.

To answer this problem we study a hybrid nanoribbon by separating a nanoribbon into two parts, one in the CDW phase and the other in the AF phase: See Fig.1(d). Only the \mathcal{C}_v and

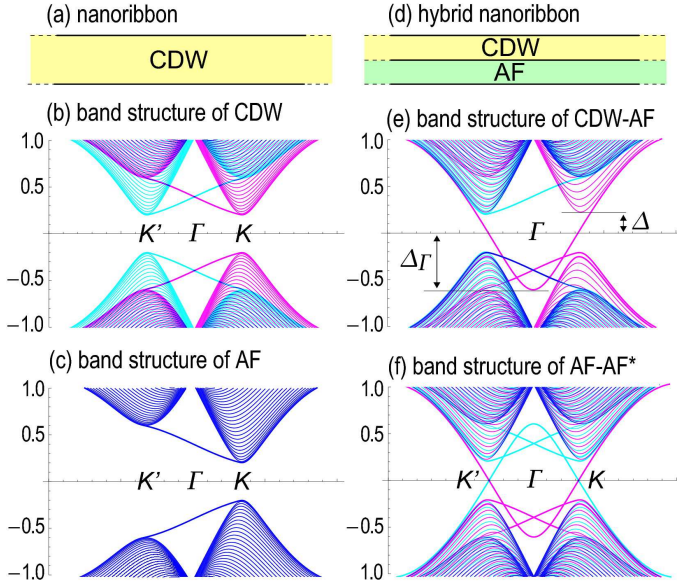


FIG. 1: (Color online) Illustration of (a) a nanoribbon and (d) a hybrid nanoribbon. Band structure of nanoribbon made of (b) CDW and (c) AF insulators. Band structure of a hybrid nanoribbon made of (e) CDW-AF, and (f) AF-AF* insulators. Up(down)-spin bands are shown in magenta (cyan). We have taken $\lambda_{SO} = 0.2t$, $\lambda_V = 0.4t$ and $\lambda_{SX} = 0.4t$ unless zero for illustration.

C_{sv} numbers change across the boundary separating these two regions. We have calculated the band structure of such a hybrid nanoribbon, whose result we display in Fig.1(e). We find one edge state crossing the Fermi energy twice. It is a manifestation of the fact that the C and C_s numbers do not change. On the other hand, when we concentrate on the vicinity of the K and K' points, there are well defined edge states. It is a manifestation of the fact that the C_v and C_{sv} numbers change at the junction.

We proceed to argue how strongly the C_v and C_{sv} numbers are protected. The word "topologically protected" means that the edge states are robust against perturbations whose magnitude is less the bulk gap Δ . Indeed, the bulk gap may close by perturbations stronger than it, invalidating the topological arguments at all. How robust is the edge mode at the CDW-AF junction? We have checked that the edge mode takes the extremal energy Δ_Γ at the Γ point with

$$|\Delta_\Gamma| = t - \lambda_V - \lambda_{SX}. \quad (9)$$

It costs the energy Δ_Γ to remove the edge states. Now, the topological edge states are protected by the bulk energy gap

$$\Delta = |\eta s_z \lambda_{SO} - \lambda_V - s_z \lambda_{SX}|. \quad (10)$$

We find $\Delta_\Gamma \gg \Delta$ since Δ_Γ is the order of eV, while Δ is the order of meV. It is very robust against perturbations.

AF-AF* junction: The second example is given by the junction made of AF with $(0, 0, 0, 2)$ and AF* with $(0, 0, 0, -2)$. The phase boundary is an antiferromagnetic domain wall with the magnetization reversed at a line defect. Let

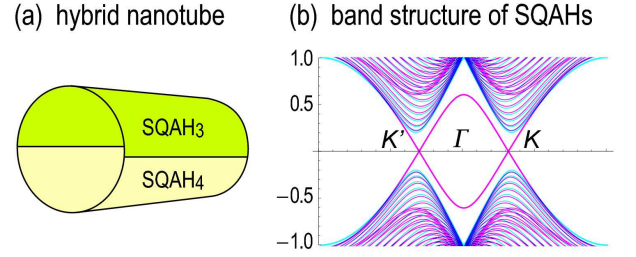


FIG. 2: (Color online) (a) Illustration of a hybrid nanotube. (b) Band structure of a hybrid nanotube made of SQA_{H1} and SQA_{H2}. Up(down)-spin bands are shown in magenta (cyan). We have taken $\lambda_{SO} = \lambda_V = \lambda_{SX} = 0.2t$ for illustration.

us take the line along the x axis. The junction is created by introducing the order parameter such that $\lambda_{SX}(y) = \lambda_{SX}$ for $y > 0$ and $-\lambda_{SX}$ for $y < 0$. To investigate the edge state located at $y = 0$, we calculate the band structure of a hybrid nanoribbon composed of the AF phase and the AF* phase. We present the result in Fig.1(f). We see clearly gapless edge modes highly enhanced at the Γ point. The extremal energy Δ_Γ of the gapless edge mode is given by (9), while the bulk gap is given by (10) also in this case. The edge is very robust.

SQAH-SQAH junction: We next investigate the junction made of two different SQAHs. As an explicit example we take SQA_{H1} with $(C, C_s, C_v, C_{sv}) = (1, 1, 1, -1)$ and SQA_{H2} with $(1, 1, -1, 1)$. It is not appropriate to use a hybrid nanoribbon in the present case since gapless edge modes appear even for a simple nanoribbon in the SQAH phase. We calculate the band structure of a nanotube geometry since no gapless edge modes appear even for a simple nanotube in the SQAH phase owing to the lack of the edge itself. We take a hybrid nanotube where one half of the nanotube is SQA_{H1} and the other half is SQA_{H2}, as illustrated in Fig.2(a). We show the result in Fig.2(b), where we see clearly a gapless edge mode highly enhanced at the Γ point. The extremal energy Δ_Γ of the gapless edge mode is given by (9), while the bulk gap is given by (10) also in this case. The edge is very robust as well.

Gapless edge mode in Dirac theory: We proceed to construct the Dirac theory of the gapless edge states[26]. They emerge along a curve where the Dirac mass vanishes, $\Delta_{s_z}^\eta(x, y) = 0$. Let us take the edge along the x axis. The zero modes emerge along the line determined by $\Delta_{s_z}^\eta(y) = 0$, when $\Delta_{s_z}^\eta(y)$ changes the sign. We may set $k_x = \text{constant}$ due to the translational invariance along the x axis. We seek the zero-energy solution by setting $\psi_B = i\xi\psi_A$ with $\xi = \pm 1$. Here, ψ_A is a two-component amplitude with the up spin and down spin, $\psi_A = (\psi_A^\uparrow, \psi_A^\downarrow)$. Setting $\psi_A(x, y) = e^{ik_x x} \phi_A(y)$, we obtain $H_\eta \psi_A(x, y) = E_{\eta\xi} \psi_A(x, y)$, together with a linear dispersion relation $E_{\eta\xi} = \eta\xi \hbar v_F k_x$. We can explicitly solve this as

$$\phi_A^{s_z}(y) = C \exp \left[\frac{\xi}{\hbar v_F} \int^y \Delta_{s_z}^\eta(y') dy' \right], \quad (11)$$

where C is the normalization constant. The sign ξ is determined so as to make the wave function finite in the limit $|y| \rightarrow$

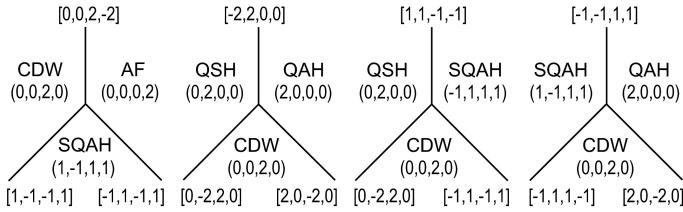


FIG. 3: Illustrations of typical Y-junctions. The edge between two different topological insulators carries a set of four topological charges. Three edges can make a Y-junction provided that the sum of their topological charges is zero.

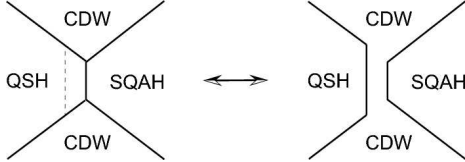


FIG. 4: Schematic illustration of topological electronic circuit. The CDW phase is created by applying electric field E_z to the QSH phase beyond the critical value E_{cr} . Tuning it locally we can change the form of circuit by a pair annihilation of two Y-junctions.

∞ . This is a reminiscence of the Jackiw-Rebbi mode[33] presented for the chiral mode. The difference is the presence of the spin and valley indices in the wave function.

Topological Kirchhoff law: We consider a configuration where three different topological insulators meet at one point: See Fig.3. In this configuration there are three edges forming a Y-junction. It is convenient to assign the topological numbers to each edge which are the difference between those of the two adjacent topological insulators. Namely, when the topological insulator with $(\mathcal{C}^L, \mathcal{C}_s^L, \mathcal{C}_v^L, \mathcal{C}_{sv}^L)$ is on the left-hand side of the one with $(\mathcal{C}^R, \mathcal{C}_s^R, \mathcal{C}_v^R, \mathcal{C}_{sv}^R)$, we assign the numbers $[\mathcal{C}^L - \mathcal{C}^R, \mathcal{C}_s^L - \mathcal{C}_s^R, \mathcal{C}_v^L - \mathcal{C}_v^R, \mathcal{C}_{sv}^L - \mathcal{C}_{sv}^R]$ to the boundary, as illustrated in Fig.3. The condition which edges can make a Y-junction is the conservation of these topological numbers at the junction. This law is a reminiscence of the Kirchhoff law, which dictates the conservation of currents at the junction of electronic circuits. We call it the topological Kirchhoff law.

The number of Y-junctions is given by the combination of selecting 3 from 16 topological insulators, i.e., ${}_{16}C_3 = 560$. The number of topological edge states is determined by the combination of selecting 2 from 16 topological insulators. We have ${}_{16}C_2 = 120$ types of topological edge states. We show typical examples of Y-junctions in Fig.3.

We present an interesting interpretation of the topological Kirchhoff law. We may regard each topological edge state as a world line of a particle carrying the four topological charges. The Y-junction may be interpreted as a scattering process of these particles. In this scattering process, the topological charges conserve.

Topological electronic circuits: We can construct electronic circuits made of edge states by joining Y-junctions. Each topological edge state carries conductance[34], whose

magnitude is given by the Chern number \mathcal{C} in unit of e^2/h . In general, the edge states carry charge \mathcal{C} , spin \mathcal{C}_s , valley-charge \mathcal{C}_v and spin-valley-charge \mathcal{C}_{sv} . The present-day electronic circuits only use the charge degree of freedom. In our circuits of topological edges we can make a full use of four types of charges. This would greatly enhance the ability of information processing.

We can control the position of edge state by controlling the parameters of the bulk states. The easiest way is to apply electric field E_z locally. Let us review the topological phase transition taking place as E_z changes[26] by taking $\lambda_\Omega = \lambda_{SX} = 0$, where the Dirac mass is given by $\Delta_{s_z}^\eta = \eta s_z \lambda_{SO} - \ell E_z$. The condition $\Delta_{s_z}^\eta = 0$ implies $E_z = \pm E_{cr}$ with $E_{cr} = \lambda_{SO}/\ell$. It follows that $(\mathcal{C}, \mathcal{C}_s) = (0, 0)$ for $|E_z| < E_{cr}$ and $(0, \frac{1}{2})$ for $|E_z| > E_{cr}$. For instance, the two CDW domains are made in this way in Fig.4(a). Applying E_z only to a part in the QSH domain near the SQAHA domain, we can turn this part into the CDW domain as in Fig.4(b). We have thus changed the form of circuit by a pair annihilation of two Y-junction by applying E_z . This will open a way to topological electronics.

I am very much grateful to N. Nagaosa for many fruitful discussions on the subject. This work was supported in part by Grants-in-Aid for Scientific Research from the Ministry of Education, Science, Sports and Culture No. 22740196.

-
- [1] M.Z Hasan and C. Kane, Rev. Mod. Phys. **82**, 3045 (2010).
 - [2] X.-L. Qi and S.-C. Zhang, Rev. Mod. Phys. **83**, 1057 (2011).
 - [3] E. Prodan, Phys. Rev. B **80**, 125327 (2009).
 - [4] D. N. Sheng, Z. Y. Weng, L. Sheng and F. D. M. Haldane, Phys. Rev. Lett. **97** 036808 (2006).
 - [5] Y. Yang, Z. Xu, L. Sheng, B. Wang, D.Y. Xing, and D. N. Sheng, Phys. Rev. Lett. **107**, 066602 (2011).
 - [6] A. Rycerz, J. Tworzydo and C. W. J. Beenakker, Nature Physics, **3**, 172 (2007).
 - [7] Z. Qiao, S. A. Yang, W. Feng, W.-K. Tse, J. Ding, Y. Yao, J. Wang, and Q. Niu, Phys. Rev. B **82**, 161414 R (2010).
 - [8] Z. Qiao, Y. Yao, S. A. Yang, B. Wang, Q. Niu, Phys. Rev. B **84**, 035431 (2011).
 - [9] Z. Qiao, H. Jiang, X. Li, Y. Yao, Q. Niu, Phys. Rev. B **85**, 115439 (2012).
 - [10] Z. Qiao, X. Li, W.-K. Tse, H. Jiang, Y. Yao, Q. Niu, Phys. Rev. B **87**, 125405 (2013).
 - [11] D. Xiao, W. Yao, and Q. Niu, Phys. Rev. L **99**, 236809 (2007).
 - [12] D. Xiao, G.-B. Liu, W. Feng, X. Xu, W. Yao, Phys. Rev. Lett. **108**, 196802 (2012).
 - [13] T. Cao, J. Feng, J. Shi, Q. Niu, E. Wang, Nat. Com. **3**, 887 (2012).
 - [14] J. Jung, F. Zhang, Z. Qiao, A. H. MacDonald, Phys. Rev. B **84**, 075418 (2011).
 - [15] W. Yao, D. Xiao, Q. Niu, Phys. Rev. B **77**, 235406 (2008).
 - [16] W.-K. Tse, Z. Qiao, Y. Yao, A. H. MacDonald, Q. Niu, Phys. Rev. B **83**, 155447 (2011).
 - [17] J. Ding, Z. Qiao, W. Feng, Y. Yao, and Q. Niu, Phys. Rev. B **84**, 195444 (2011).
 - [18] F. Zhang, J. Jung, G. A. Fiete, Q. Niu, and A. H. MacDonald, Phys. Rev. Lett. **106**, 156801 (2011).
 - [19] F. Zhang, A. H. MacDonald, and E. J. Mele, Proc. Natl. Acad.

- Sci. USA 110, 10546 (2013).
- [20] J. Li, A. F. Morpurgo, M. Büttiker, and I. Martin, Phys. Rev. B 82, 245404 (2010).
- [21] M. Ezawa, Phys. Rev. B 87, 155415 (2013).
- [22] M. Ezawa, Phys. Rev. Lett **109**, 055502 (2012).
- [23] M. Ezawa, Phys. Rev. Lett. **110**, 026603 (2013).
- [24] C. L. Kane and E. J. Mele, Phys. Rev. Lett. **95**, 226801 (2005).
- [25] C.-C. Liu, H. Jiang, and Y. Yao, Phys. Rev. B **84**, 195430 (2011).
- [26] M. Ezawa, New J. Phys. **14**, 033003 (2012).
- [27] F. D. M. Haldane, Phys. Rev. Lett. **61**, 2015 (1988).
- [28] X. Li, T. Cao, Q. Niu, J. Shi, and J. Feng, PNAS 110 3738 (2013).
- [29] T. Kitagawa, T. Oka, A. Brataas, L. Fu, and E. Demler, Phys. Rev. B 84, 235108 (2011).
- [30] T. Oka and H. Aoki, Phys. Rev. B 79, 081406(R) (2009).
- [31] Q.-F. Liang, L.-H. Wu, X. Hu, New J. Phys. 15 063031 (2013).
- [32] M. Ezawa, Euro. Phys. J. B **85**, 363 (2012).
- [33] R. Jackiw and C. Rebbi, Phys. Rev. D **13**, 3398 (1976).
- [34] M. Ezawa, Appl. Phys. Lett. **102**, 172103 (2013).